PHYSICS OF FLUIDS **27**, 033602 (2015)

Start-up vortex flow past an accelerated flat plate

Ling Xu[1,a)] and Monika Nitsche[2,b)]
[1]*Department of Applied and Computational Mathematics and Statistics, University of Notre Dame, Notre Dame, Indiana 46556, USA*
[2]*Department of Mathematics and Statistics, University of New Mexico, Albuquerque, New Mexico 87131, USA*

(Received 20 April 2014; accepted 11 January 2015; published online 11 March 2015)

Viscous flow past a finite flat plate accelerating in the direction normal to itself is studied numerically. The plate moves with nondimensional speed t^p, where $p = 0, 1/2, 1, 2$. The work focuses on resolving the flow at early to moderately large times and determining the dependence on the acceleration parameter p. Three stages in the vortex evolution are identified and quantified. The first stage, referred to as the Rayleigh stage [Luchini and Tognaccini, "The start-up vortex issuing from a semi-infinite flat plate," J. Fluid Mech. **455**, 175–193 (2002)], consists of a vortical boundary layer of roughly uniform thickness surrounding the plate and its tip, without any separating streamlines. This stage is present only for $p > 0$, for a time-interval that scales like p^3, as $p \to 0$. The second stage is one of self-similar growth. The vortex trajectory and circulation satisfy inviscid scaling laws, the boundary layer thickness satisfies viscous laws. The self-similar trajectory starts immediately after the Rayleigh stage ends and lasts until the plate has moved a distance $d = 0.5$ to 1 times its length. Finally, in the third stage, the image vorticity due to the finite plate length becomes relevant and the flow departs from self-similar growth. The onset of an instability in the outer spiral vortex turns is also observed, however, at least for the zero-thickness plate considered here, it is shown to be easily triggered numerically by underresolution. The present numerical results are compared with experimental results of Pullin and Perry ["Some flow visualization experiments on the starting vortex," J. Fluid Mech. **97**, 239–255 (1980)], and numerical results of Koumoutsakos and Shiels ["Simulations of the viscous flow normal to an impulsively started and uniformly accelerated flat plate," J. Fluid Mech. **328**, 177–227 (1996)]. © *2015 AIP Publishing LLC.* [http://dx.doi.org/10.1063/1.4913981]

I. INTRODUCTION

This paper presents numerical simulations of the starting vortex flow at the edge of an accelerating finite flat plate. The plate is assumed to have zero thickness and moves in the direction normal to itself with speed $a\hat{t}^p$, where a is a dimensional constant and $\hat{t}$ has units of time. The flow is nondimensionalized based on the plate length and the parameter a, yielding a characteristic flow Reynolds number Re. We study the effect of the acceleration parameter p for fixed value of Re.

Of intrinsic interest in fluid dynamics, the starting vortex flow has been the focus of much research, beginning with the work of Prandtl in 1904.[1,2] Most directly relevant to the accelerating case considered here are the laboratory experiments of Taneda and Honji,[3] and Pullin and Perry,[4] and the numerical results of Koumoutsakos and Shiels.[5] Taneda and Honji[3] observed a scaling of the vortex size for flow past a thin plate. Pullin and Perry[4] reported detailed measurements of the vortex trajectory for flow past a wedge, for a range of acceleration parameters p and wedge angles as small as 5°, and compared their observations to inviscid similarity theory.[6,7] Their results are

a)Electronic mail: xulingsue@gmail.com
b)Electronic mail: nitsche@math.unm.edu

close to planar and provide a good basis of comparison for our work. More recent experiments address leading edge flow onto a plate and three-dimensional tip vortex effects (Kriegseis, Kinzel and Rival,[8] Ringuette, Milano and Gharib[9]). Koumoutsakos and Shiels[5] presented numerical results for flow past a plate of zero thickness moving with either impulsively started velocity ($p = 0$) or constant acceleration ($p = 1$) and reported vorticity distributions at relatively large times.

The present paper complements these earlier works with simulations of the flow over a range of early to intermediate times, for several values of p. The main contributions are to resolve the early time flow, to compute and resolve the trajectory and circulation over a large range of times, and to report new features of the flow for $p > 0$ which are not present for $p = 0$. Most results presented are for varying p with fixed Reynolds number $Re = 500$. The effect of Reynolds number for fixed $p = 0$ is presented elsewhere.[10] The flow is difficult to compute because of the singular geometry. We use a split method in time in which advection is treated using a semi-Lagrangian scheme, diffusion is treated with a three-level Crank-Nicholson method, and all finite difference and interpolation approximations are of fourth order. The convergence of the method is documented to be approximately of second order, and the results validated by comparing with the available experimental and numerical data in Refs. 3–5.

At early times, the size of the starting vortex is small relative to the plate length, which suggests that the flow behaves locally as in the absence of an external length scale. In that case, the scaling of the flow can be investigated using dimensional analysis. Different results are obtained for inviscid and for viscous flow. Pullin[7] considered an inviscid asymptotic vortex sheet model for start-up flow past a semi-infinite plate and derived inviscid scaling laws for the vortex center trajectory and circulation. He then computed the time-independent self-similar vortex sheet shape and quantified the magnitude of the inviscid self-similar growth. In the presence of viscosity, dimensional analysis yields scaling laws for the boundary and shear layer thicknesses, velocities, and vorticities. The viscous scaling was exploited by Luchini and Tognaccini,[11] who computed viscous flow past a semi-infinite plate in a self-similar reference frame. Here, we investigate the extent to which the viscous and inviscid scaling holds for the accelerated flow. The results can be formulated in the framework proposed by Luchini and Tognaccini[11] for the starting vortex evolution. They described four stages in the evolution: a first Rayleigh stage in which the flow consists solely of a viscous vortical boundary layer around the plate and its tip; a second viscous stage in which convective terms in the Navier-Stokes equations are comparable to the viscous terms and a vortex structure appears; a third stage in which convection dominates, but the length scales are still small so that the vortex grows according to inviscid self-similar scaling laws; and a fourth stage in which the plate geometry is no longer negligible and significantly affects the flow. Our computations enable us to quantify this description. We find that the Rayleigh stage, which ends with the formation of a recirculation region, is only present for $p > 0$ and lasts for a time that scales as p^3. The self-similar regime begins immediately at the end of the Rayleigh stage. In this regime, the vortex trajectory and circulation satisfy inviscid scaling laws, and the boundary layer thickness grows according to viscous scaling. The self-similar stage ends when the plate has moved by about $d = 0.5$ to 1 times the plate length, depending on the value of p. After this time, the finite plate length is no longer negligible and significantly affects the flow. From our present results, we have therefore little indication of a distinct viscous stage in between the Rayleigh stage and the self-similar regime.

An aspect of the start-up flow much studied in the literature is the onset of a shear layer instability in the outer spiral vortex turns, reported, for example, in the experiments of Pierce[12] and Lian and Huang.[13] Wang, Liu and Childress[14] compute flow past a smooth elliptical plate and resolve stream function oscillations near the plate tip that result in unstable shear layer rollup. Also using simulations, Schneider *et al.*[15] find a connection between the starting vortex instability and the shape of the plate tip. Lepage, Leweke and Verga[16] performed experiments of the starting vortex at the edge of a rotating blade and compute the strain rate along the separated shear layer. They suggest that the observed non-monotonicity of the strain rate may lead to loss of stability in the outer shear layer turns. Here, we show that at least for flow past a zero thickness plate, the instability is easily triggered numerically by underresolution.

The paper is organized as follows. Sections II and III present the problem and the numerical method used, Sec. IV presents the numerical results, and Sec. V summarizes the observations.

II. PROBLEM FORMULATION

A finite plate of length L and zero thickness, immersed in a homogeneous viscous fluid, is accelerated in the direction normal to itself with speed

$$\widehat{U} = a\widehat{t}^{\,p}, \tag{1}$$

where a is a dimensional constant. Here and throughout the paper, the hat symbol denotes dimensional variables. We consider $p = 0, 1/2, 1, 2$. These include impulsively started flow ($p = 0$), uniform acceleration ($p = 1$), and linear acceleration ($p = 2$). The flow is assumed to be two-dimensional and to remain symmetric about the centerline at all times. We choose a reference frame fixed on the plate, in which the plate is horizontal and the driving velocity moves upwards, approaching parallel flow in the far field. Figure 1 illustrates the vorticity some time after the beginning of the motion. As fluid moves from upstream (below the plate) to downstream (above the plate), boundary layers of vorticity form along the plate walls which eventually separate and form a pair of counterrotating vortices. The results are the same, up to a translation, as those for a moving plate in a reference frame fixed at infinity.

The flow is nondimensionalized with respect to the plate length and the parameter a, yielding a characteristic timescale

$$T = \left(\frac{L}{a}\right)^{1/(p+1)}, \tag{2}$$

and flow Reynolds number

$$Re = \frac{L^2}{\nu T} = \frac{a^{1/(p+1)}L^{(2p+1)/(p+1)}}{\nu}, \tag{3}$$

where ν is the kinematic fluid viscosity. The problem is described in nondimensional time t and Cartesian coordinates (x, y), chosen so that the plate lies on the x-axis, centered at the origin, at $\{(x,0) \mid x \in [-1/2, 1/2]\}$. The fluid velocity and scalar vorticity are $(u(x, y, t), v(x, y, t))$ and $\omega(x, y, t)$. The relation between dimensional and nondimensional variables is, for example,

$$t = \frac{\widehat{t}}{T}\,,\ x = \frac{\widehat{x}}{L}\,,\ U = \frac{\widehat{U}T}{L}\,,\ \omega = \widehat{\omega}T\,. \tag{4}$$

The nondimensional far field velocity is $(0, t^p)$. In a reference frame fixed at infinity, the plate moves downwards and has been displaced at time t by a distance $d = t^{p+1}/(p + 1)$. Many results herein will be shown in terms of the displacement d.

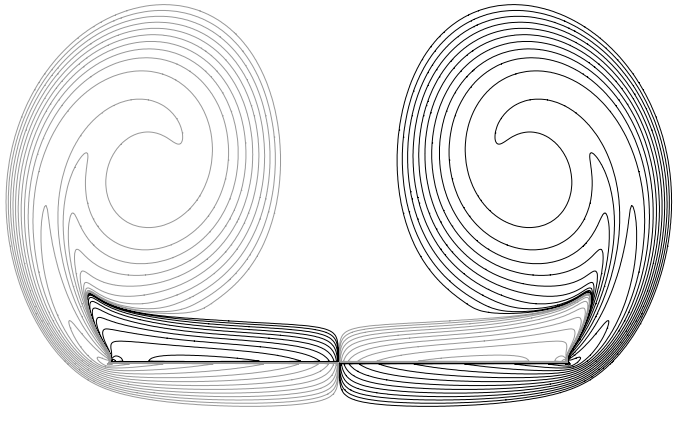

FIG. 1. Sample vorticity contours for $p = 1$ at a relatively large time, with positive vorticity in black, negative vorticity in grey.

The flow is governed by the incompressible Navier-Stokes equations,

$$\frac{D\omega}{Dt} = \frac{1}{Re}\nabla^2\omega, \quad \nabla^2\psi = -\omega, \quad (u, v) = \left(\frac{\partial\psi}{\partial y}, -\frac{\partial\psi}{\partial x}\right), \tag{5}$$

where $\frac{D}{Dt} = \frac{\partial}{\partial t} + u\frac{\partial}{\partial x} + v\frac{\partial}{\partial y}$. It is initially irrotational, $\omega(x, y, 0) = 0$, with boundary conditions $\psi = 0$, $u = 0$, and $v = 0$ on the plate, and $\psi(x, y, t) \to \psi_\infty$ as $|(x, y)| \to \infty$. Here, ψ_∞ is the potential flow that induces the far field velocity, given by the complex potential

$$\psi_\infty(x, y, t) = Im\left(t^p\sqrt{\frac{1}{4} - z^2}\right), \tag{6}$$

where $z = x + iy$.

III. NUMERICAL METHOD

Governing equations (5) are solved in a finite rectangular domain in the right half-plane, $[0, x_{max}] \times [y_{min}, y_{max}]$, using a time-splitting mixed finite-difference and semi-Lagrangian scheme. The space-time domain is discretized using a uniform mesh in space, $\Delta x = \Delta y = h$ with constant timestep Δt, over given time intervals. All spatial approximations used are of 4th order in h. The solution is advanced from time t_n to t_{n+1} by first convecting the current vorticity with the current velocity according to

$$\frac{D\omega}{Dt} = 0, \tag{7}$$

using a semi-Lagrangian scheme. The updated interior vorticity is used to compute updated boundary and interior stream function values, and then, velocity and boundary vorticity. The boundary stream function is obtained by integrating the interior vorticity with a domain-specific Green's function for the Laplace operator. The interior stream function is obtained by solving the Poisson equation in (5) with a finite difference scheme. The boundary vorticity on the plate is obtained from the interior stream function by approximating the Poisson equation at the wall so that the no-slip condition is satisfied. This is known as Briley's formula.[17] This approach is taken at the plate tip as well. Finally, we solve

$$\frac{\partial\omega}{\partial t} = \frac{1}{Re}\nabla^2\omega, \tag{8}$$

using an implicit Crank-Nicolson method. Further details are given in Xu and Nitsche[10] and Xu.[18]

Table I lists all parameters used in the present computations for various values of p. In several cases, in order to compute the flow to large times, the computations were performed using a fine mesh until some early time, subsampling that result and continuing on a coarser mesh, and repeating this process. The time intervals used are indicated in the table. For example, the result for $p = 1$ at $t = 4$ is obtained using $h = 1/1280$ for $t \in [0, 0.1]$, subsampling the result at $t = 0.1$ to continue with $h = 1/640$ until $t = 0.7$, etc.

TABLE I. List of numerical parameters: mesh size h, time step Δt, starting/ending time $t_{\text{start}}/t_{\text{end}}$, computational domain $[0, x_{\max}]\times[y_{\min}, y_{\max}]$, number of grid points $N_x \times N_y$, acceleration parameter p, and Reynolds number Re.

h	Δt	$[t_{\text{start}}, t_{\text{end}}]$	$[0, x_{\max}]\times[y_{\min}, y_{\max}]$	$N_x \times N_y$	p	Re
1/5120	2×10^{-6}	[0, 0.0004]	$[0, 0.55] \times [-0.05, 0.1]$	2816×768	0	500
1/2560	4×10^{-6}	[0, 0.005]	$[0, 0.55] \times [-0.05, 0.1]$	1408×384	0	500
1/1280	5×10^{-5}	[0, 0.1]	$[0, 0.75] \times [-0.125, 0.25]$	960×480	0, 1/2, 1, 2	500
1/640	1×10^{-4}	[0.1, 0.7]	$[0, 1.0] \times [-0.25, 0.75]$	640×640	0, 1/2, 1, 2	500
1/320	2×10^{-4}	[0.7, 3]	$[0, 1.5] \times [-0.25, 2.75]$	480×960	0, 1/2, 1, 2	500
1/160	4×10^{-4}	[3, 4]	$[0, 1.5] \times [-0.5, 5.5]$	240×960	0	500
1/1280	5×10^{-5}	[0, 0.57]	$[0, 0.75] \times [-0.1, 0.4]$	960×640	0.45	6000

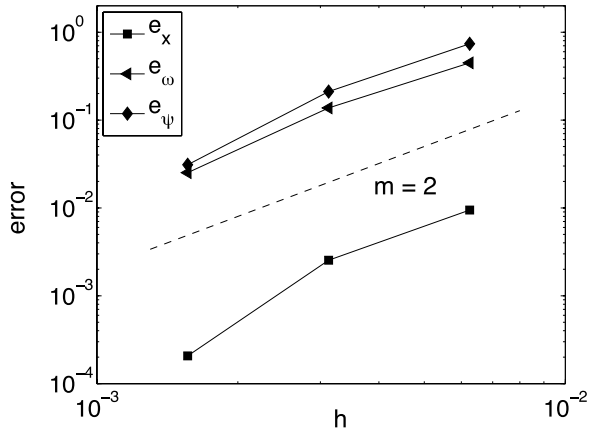

FIG. 2. Pointwise errors e_x, e_ω, e_ψ at the center of rotation, in the solution at $t = 0.3$, with $p = 1$, $Re = 500$, computed with $h = 1/160$, $h = 1/320$, $h = 1/640$, relative to the solution computed with $h = 1/1280$.

To illustrate the spatial rate of convergence of the method for the accelerated flow, Figure 2 plots the errors

$$e_{\mathbf{x}}^h = \frac{\|\mathbf{x}_c^h - \mathbf{x}_c^{h_f}\|_2}{\|\mathbf{x}_c^{h_f}\|_2}, \; e_\omega^h = \frac{|\omega_c^h - \omega_c^{h_f}|}{|\omega_c^{h_f}|}, \; e_\psi^h = \frac{|\psi_c^h - \psi_c^{h_f}|}{|\psi_c^{h_f}|}, \tag{9}$$

where $\mathbf{x}_c^h$ is the position of the center of rotation of the starting vortex at $t = 0.3$, for $p = 1$, $Re = 500$, computed with constant meshsize h. The values ω_c^h, ψ_c^h are the vorticity and stream function at that point. The figure plots the results for $h = 1/160, 1/320, 1/640$, using $h_f = 1/1280$ as the reference values. The dashed line has slope 2, indicating better than second order convergence of the results shown. Even though all spatial approximations used are of fourth order, the results are of approximately second order because of the singular plate geometry.

We note that the results are not highly sensitive to the treatment of the plate tip. For example, an alternative is to set the tip vorticity to be $\omega_{tip} = 0$, since that may be assumed to be the exact solution. This approach also yields converging results, although with slightly lower rate of convergence.

To compare with experiments, we also compute particle streaklines by releasing a material particle into the flow near the plate tip at each timestep and convecting it with the fluid velocity.

IV. NUMERICAL RESULTS

This section presents the evolution of the flow for fixed p at a sequence of times, followed by the dependence on p at a fixed displacement d. The evolution for $p = 0.45$ is compared with experiments of Pullin and Perry.[4] We then present various aspects of the evolution, such as the Rayleigh layer, differences in the emergence of the rotation center and the core vorticity maximum, and the inviscid and viscous scalings observed. Finally, the vortex size is compared with numerical results of Koumoutsakos and Shiels.[5]

A. Vorticity, streamlines, and streaklines for $p = 1$

Figure 3 presents the computed flow evolution for $p = 1$ and $Re = 500$. The figure shows vorticity contours (left), streaklines (middle), and streamlines (right) at $t = 0.04, 0.2, 0.5, 1, 1.5, 2$. Positive vorticity contours are shown in black, negative ones in grey. Results are plotted in the right half-plane, $x \geq 0$. By symmetry, the vorticity and stream function in $x \leq 0$ are of equal magnitude but opposite sign.

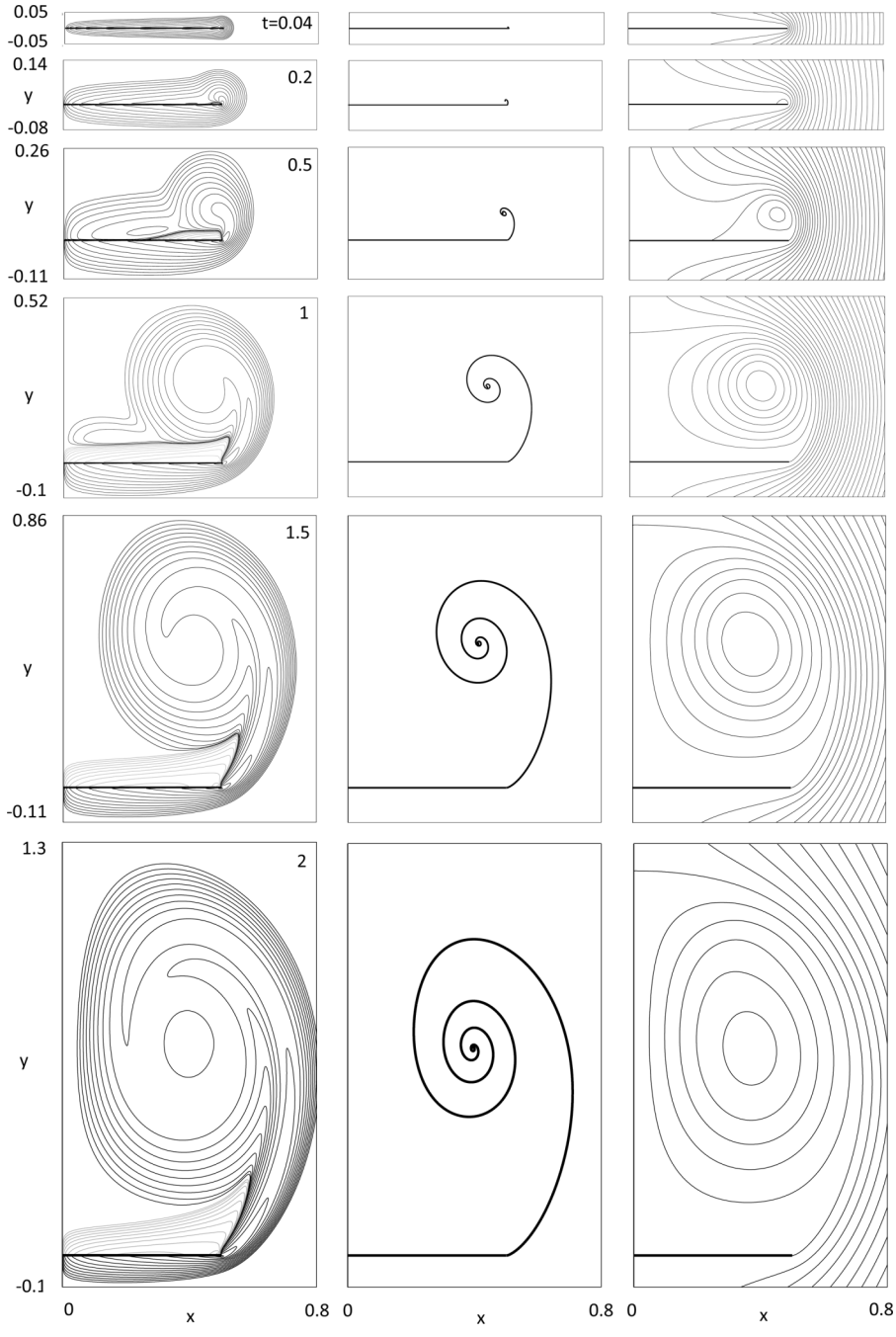

FIG. 3. Vorticity (*left*), streaklines (*middle*), and streamlines (*right)* at $t = 0.04, 0.2, 0.5, 1, 1.5, 2$, for $p = 1$, $Re = 500$. Vorticity contour levels are $\pm 2^j$, $j = -5, \ldots, 12$.

Initially, the background flow has zero velocity. As the motion begins, boundary layers of positive vorticity form around the plate, on both the upstream side (below) and downstream side (above). This early vorticity is almost symmetric across the plate, as seen in Figure 3 at $t = 0.04$. The corresponding streamlines, in the right column, are also practically symmetric across the plate. As time evolves, upstream vorticity is convected downstream, concentrating near the tip and breaking the initial symmetry. A region of recirculating flow forms around the vorticity concentration, bounded by the zero level streamline. This streamline follows the plate, leaves at the tip to surround

the vortex core, and reattaches to the plate at early times. At later times, it reaches the symmetry axis. The recirculation region is seen as early as $t = 0.2$ in Figure 3, in the right column. In Sec. IV D, we show that it first appears around $t = 0.1$. Within the recirculation region, the reversed flow direction at the wall induces a boundary layer of opposite signed negative vorticity. As time evolves, the upstream positive boundary layer vorticity continues to be convected downstream, the leading vortex grows and induces more negative boundary vorticity on the plate. Some of the negative vorticity is eventually entrained by the vortex, which convects downstream.

The streaklines shown in the middle column in Figure 3 are computed by releasing material particles from the vicinity of the plate tip at each time step and convecting them with the fluid velocity. At any given time, Figure 3 shows the current position of all particles released previously, mimicking what is visualized in laboratory experiments.[3,4] The particles rotate around the vortex center, with particles that have been released earlier traveling closer to the center than those released later, resulting in a spiral streakline shape. We note that the tip, which is the point at which the particles are released, is also the point at which the vorticity is maximal. The particle movement thus approximates the convection of the maximum vorticity, and therefore their position approximates the centerline of maximum vorticity in the separated shear layer.

Below, we will more closely address the early time formation period and the corresponding shed circulation, which have not previously been studied numerically in detail. On the other hand, much work has focused on the onset of an instability on the outer spiral shear layer turns at later times. Figure 4(a) shows an example displaying the characteristic shear layer instability. It plots the solution at $t = 5$, for $p = 1$, and $Re = 1000$, computed using constant meshsize $h = 1/80$, timestep $\Delta t = 2 \times 10^{-4}$. The result is similar to the result of Koumoutsakos and Shiels[5] presented in their figure 26(e), which they obtained for the same $t = 5$, $p = 1$, but a lower value of $Re = 400$. We recomputed the case in Figure 4(a) using a smaller meshsize $h = 1/160$, and this result is shown in Figure 4(b). Clearly, the finer mesh yields less oscillatory results, showing that the instability observed in Figure 4(a) is induced by lack of resolution. The effect of underresolution of various methods on shear-layer instability was studied in detail by Brown and Minion.[19] On the other hand, Schneider *et al.*[15] find a connection between the starting vortex instability and the shape of the plate tip, and Wang *et al.*[14] find a connection between the stream function oscillations near the tip of a smooth elliptical plate and the observed instability in that case. Our results presented here indicate

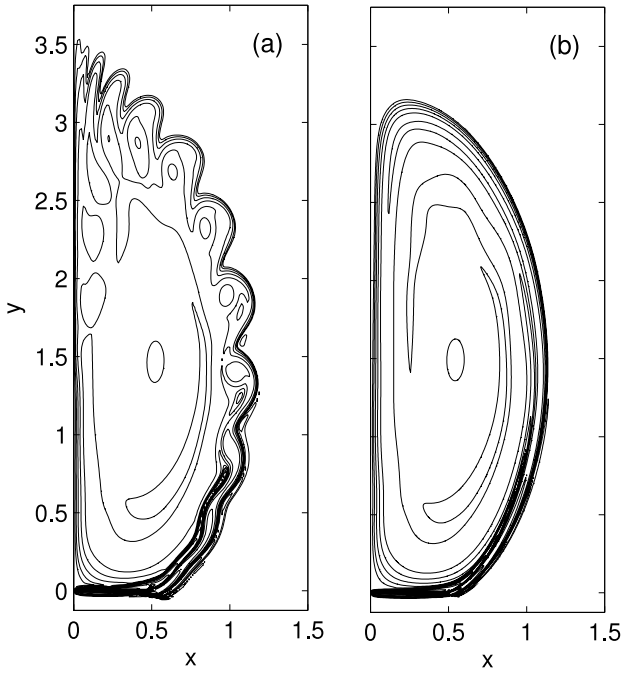

FIG. 4. Vorticity at $t = 5$, for $p = 1$ and $Re = 1000$, computed with (a) $h = 1/80$ and (b) $h = 1/160$.

that for the zero thickness plate the instability is easily triggered by underresolution. We cannot resolve the flow at large times sufficiently well to make a more conclusive statement about the instability, which is therefore out of the scope of this paper.

B. Dependence on *p* at fixed displacement *d* = 1

The parameter p describes the driving velocity $(0, t^p)$ in the far field. In a reference frame fixed at infinity, the plate moves downward with velocity $(0, -t^p)$. The solution at a fixed time t depends greatly on p since the plate has travelled significantly different distances $d = \frac{1}{p+1} t^{p+1}$, resulting in vortices of significantly different sizes. For a better evaluation, we choose to compare solutions with varying p not at equal times t, but at times of equal plate displacement d. All results shown herein are therefore plotted in reference to the displacement d instead of time t.

Figure 5 compares the vorticity profiles (top), streaklines (middle), and flow streamlines (bottom) at fixed displacement $d = 1$ for all $p = 0, 1/2, 1, 2$. As p increases, the vortex decreases slightly in size, the core vorticity becomes more uniform, and the wall boundary layer thickness decreases slightly. As p increases, the spiral streakline shapes also change. The roll-up away from the center is less tight. For larger p, more particles released at early times end up near the spiral center, since the vortex has travelled less far from the plate at these times. As p increases, the spiral shape is also more elliptical and less round. It leans further inwards, with the line from the spiral center to the plate tip subtending a smaller angle with the plate. The density of the streamlines plotted in the bottom row shows that the velocity magnitude in the vortex is largest for $p = 2$.

The vorticity and velocity profiles as a function of p are shown more clearly in Figures 6(a) and 6(b) which plot the profiles at $d = 1$ along the vertical line $x = x_m$ through the vorticity maximum (x_m, y_m) in the vortex center, as a function of y. Figure 6(a) shows that the vorticity profile is flatter

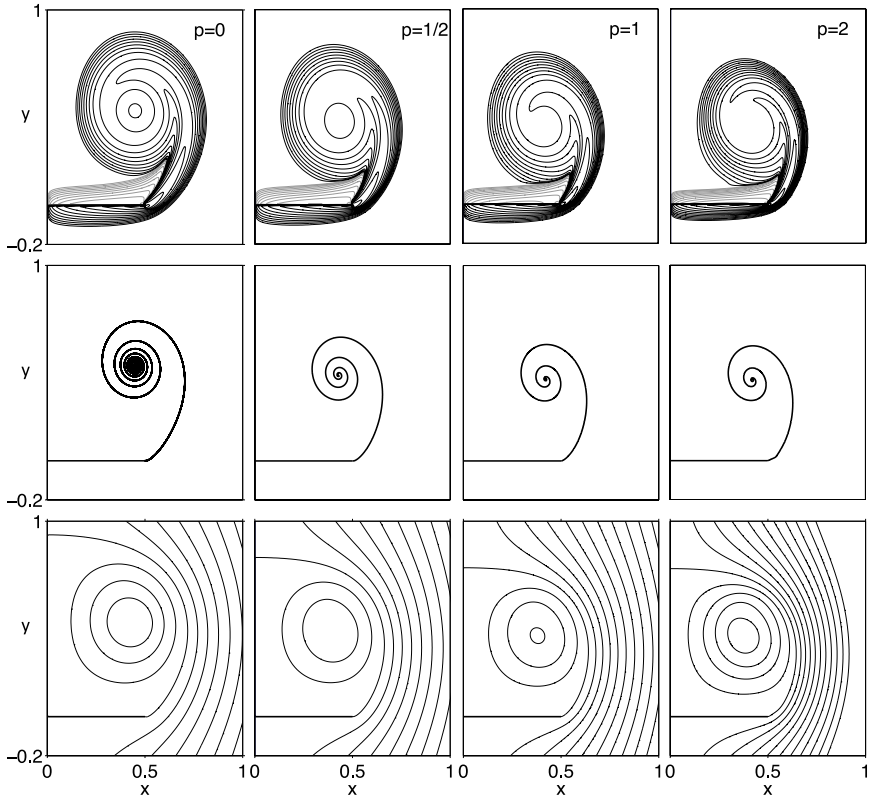

FIG. 5. Vorticity (*top*), streaklines (*middle*) and streamlines (*bottom*) for fixed displacement $d = 1$, and $p = 0, 1/2, 1, 2$, as indicated.

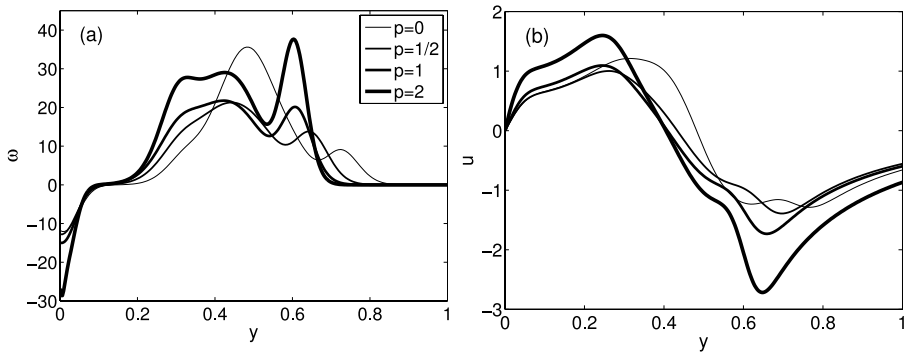

FIG. 6. (a) Vorticity and (b) velocity at $d = 1$ along a vertical line $x = x_m$ through the core vorticity maximum, vs. y, for $p = 0, 1/2, 1, 2$, as indicated.

near the core for larger values of p. The outermost shear layer turn is stronger for larger p, with larger maximal vorticities that occur at a smaller value of y, reflecting the smaller shape seen in the vorticity contours. Figure 6(b) plots the horizontal velocity component u along $x = x_m$ and shows the velocity gradients in the core, which behave as deduced from Figure 5: the magnitude is largest for $p = 2$. The velocity profiles also show the decreasing y-coordinate of the point with $u = 0$, near the rotation center, as p increases.

C. Comparison with laboratory experiments

The closest experimental results available for comparison with the simulations presented in this paper are those of Pullin and Perry[4] of flow past a wedge of angle β. Their streakline visualizations for the smallest wedge angle used, $\beta = 5°$, are reproduced here in Figure 7, left column. The photographs show snapshots of an experiment performed in a rectangular tank, in which water flows from left to right past a planar wedge of height $l = 12.7$ cm attached to the top of the tank. Near the midsection of the tank, the flow is close to planar. Dye initially lines the walls of the wedge near the midsection and trickles almost vertically downward before the motion begins. The photographs show the position of the dye at the indicated dimensional times after the beginning of the flow, for (dimensional) background velocity $\widehat{U} = a\hat{t}^p$, with $p = 0.45$, $a = 0.86$ cm/s^{p+1}. By symmetry, the flow is comparable to flow past a plate with $L = 2l$. At water temperature of 24 °C, the corresponding Reynolds number as defined in Eq. (3) is $Re = 6621$.

The dye along the wall separates and rolls up into the inner spiral turns seen in the figure, while the dye that initially had trickled almost vertically downward rolls up into the outer spiral turns. The figure also shows that initially an additional drop of dye was placed in the water, to the right of the plate, slightly above the tip. This drop evolves into a third streakline that closely hugs the wall until the last time shown ($t = 5$ s), when it has moved below the tip of the plate.

The experimental results are compared with the present numerical simulations of flow past a flat plate, with $p = 0.45$ and $Re = 6000$. The computed streaklines are shown in Figure 7, middle column, at the nondimensional times corresponding to those shown in the left column. The computed results are shown in a rotated frame similar to the experimental reference frame. For better comparison, the figure also plots the position of particles initially placed along a close to vertical line below the plate (in the rotated frame) as well as particles initially forming a drop close to the drop visible in the experiments. The resulting set of streaklines is in very good agreement with the experiment. The spiral size, shape, and angle of inclination agree, as well as details of the streakline evolving from the drop. The spiral centers will be compared in more detail in Sec. IV E.

For larger wedge angles, Pullin and Perry found a second spiral streakline separating on the downstream side of the wedge at a point a short distance from the tip, indicating the formation of a secondary region of recirculation. The streamlines corresponding to the computed results in the

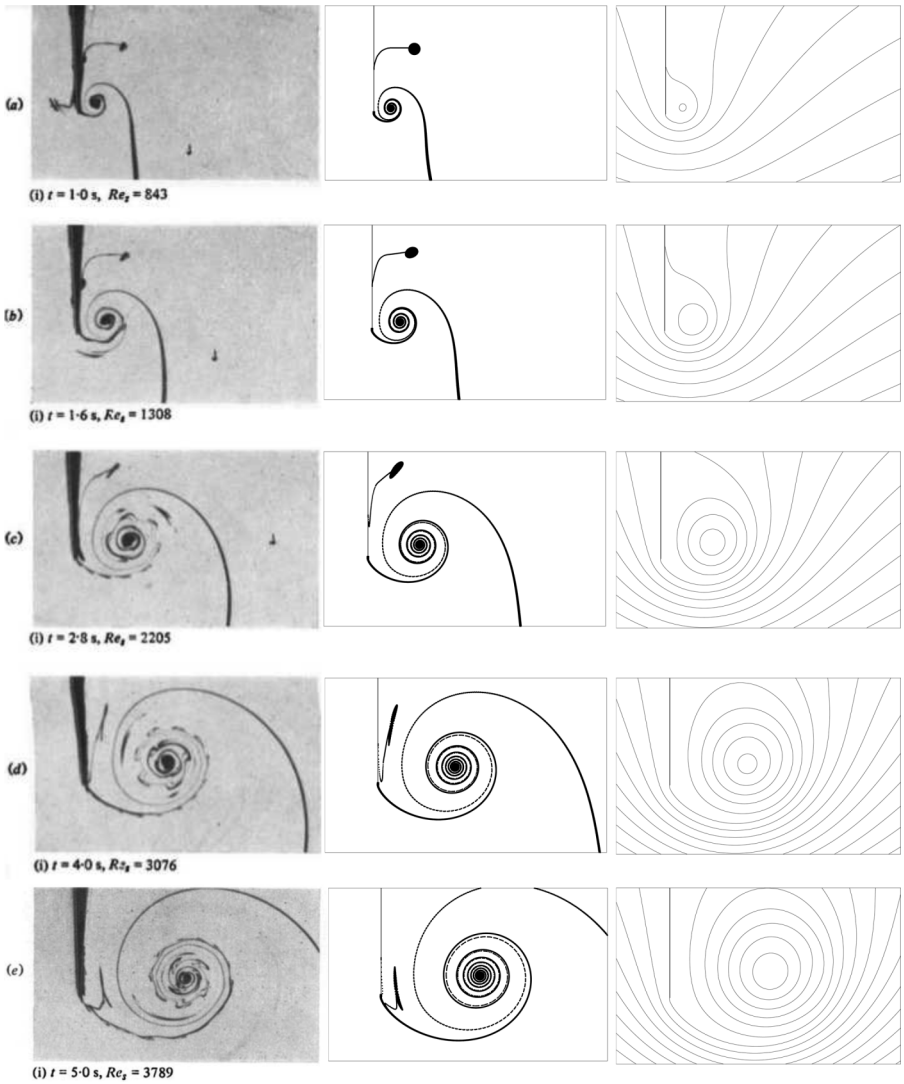

FIG. 7. Left column: Streaklines for flow past a wedge of angle $\beta = 5°$, at $t = 1$ s, 1.6 s, 2.8 s, 4 s, and 5 s, for $p = 0.45$ and $Re = 6621$, obtained by Pullin and Perry[4] from laboratory experiments. Reproduced with permission from D. I. Pullin and A. E. Perry, J. Fluid Mech. **97**, 239-255 (1980). Copyright 1980 Cambridge University Press. Middle and Right columns: Numerical simulations of streaklines and streamlines, respectively, for flow past a flat plate at the same times, for $p = 0.45$ and $Re = 6000$.

middle column, for flow past a flat plate, are shown in Figure 7, right column. They show that in this case, there is no secondary separation. They also show that the drop of dye, while initially placed outside the recirculation region, is later entrained into the vortex. The good agreement between computed and experimental streamlines indicates that in the experiment with small angle $\beta = 5°$, secondary separation is practically absent. Resolving the small scales for the $\beta > 0$ case remains an interesting topic of study.

Some differences between experiment and simulation are observed in Figure 7. In the experiment, small vortices are observed on the outer spiral turn, reflecting the shear layer instability, which is not seen in the computed results at these times. These may be caused by the finite thickness plate tip.[14,15] There are also small differences in the position of the outer spiral turn, which may be caused by differences in the initial particle positions below the plate, for which no experimental data are available.

D. Stages in the starting vortex evolution

Luchini and Tognaccini[11] propose four stages in the evolution of the starting vortex: a first Rayleigh stage in which the flow is potential everywhere except for a thin boundary layer of constant thickness around the whole plate; a second viscous stage in which convective terms in the Navier-Stokes equations are comparable to the viscous terms and a vortex structure appears; a third stage in which convection dominates, but the length scales are still small so that the vortex grows according to inviscid self-similar scaling laws; and a fourth stage in which the plate geometry is no longer negligible and significantly affects the flow. In this section and Secs. IV E–IV F, we describe the evolution observed numerically and quantify it in relation to this proposed scenario.

Various stages in the observed evolution are loosely captured in Figure 8. The figure plots vorticity contours for $p = 1/2$ at an increasing sequence of displacements (see caption). It also plots the level curve $\psi = 0$ that bounds the region of recirculating flow, as well as a streamline close to the center of rotation within this region. Figure 8(a) shows a clear and well-defined first Rayleigh stage in which the vorticity forms an almost symmetric boundary layer of uniform thickness around the plate, without any streamline separation. This stage ends at a time $t = T_R$ when a region of recirculating flow appears near the tip of the plate, with a well-defined rotation center and associated negative vorticity layer, see Figure 8(b). Numerically, T_R is defined as the time at which opposite signed wall vorticity and stream function values first appear.

Figures 8(c) and 8(d) plot the solution at later times. The main new feature here is that the vorticity has developed a local maximum in the vortex core not present in Figure 8(b). We define the time at which it appears as $t = T_M$. The position and magnitude of the rotation center and the vorticity maximum are denoted by x_c, y_c, ω_c, and x_m, y_m, ω_m, respectively, as illustrated in Figure 8(d). Their scaling behaviour is the subject of Secs. IV E and IV F. As will be seen, near the time plotted in Figure 8(d), the vortex begins to depart from the self-similar growth, and the finite plate geometry becomes significant. For later reference, Figure 8(d) also defines the height s_ψ of the recirculation region.

Figure 9 compares the trajectory of the rotation center (x_c, y_c) for $t > T_R$ (solid) and the core vorticity maximum (x_m, y_m) for $t > T_M$ (dashed) for $p = 0, 1/2, 1, 2$, computed for displacements $d \in [0, 3]$. The trajectories are plotted on a one-to-one scale, showing that the vortex travels much faster in the vertical direction away from the plate than in the horizontal direction. At first, it travels inward, with decreasing values of x, towards the axis, and after some time, it turns to travel outward. The turning will be seen later to occur at approximately $d = 1.5$, which is past the time plotted in Figure 8(d). Figure 9 shows that as p increases, the vorticity maximum appears further away from the plate tip; the difference between the maximum and the rotation center increases; the trajectory of the maximum oscillates, with increasing oscillation amplitude.

Figure 10 plots the duration T_R of the Rayleigh stage, that is, the time when the recirculation region appears, and the time T_M when the vorticity maximum appears, as functions of p, computed with three resolutions, $h = 1/320$, $1/640$, and $1/1280$. The times T_S are shown here for later reference. Two dashed lines with the indicated slopes are also shown. The values of T_M are much larger than T_R, showing that the vorticity maximum appears significantly later than the recirculation

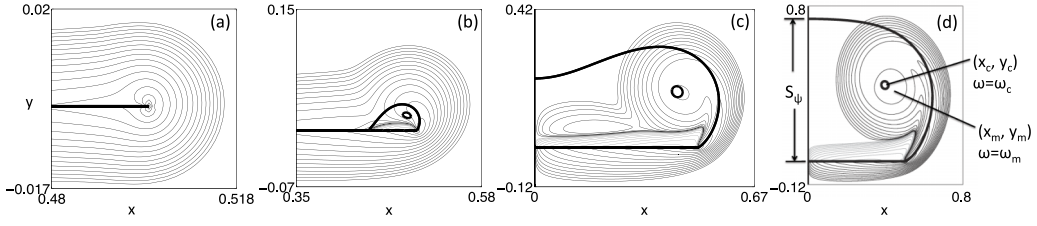

FIG. 8. Four stages in the vorticity evolution, illustrated here for $p = 1/2$, at times (a) $d = 0.000\,24$ ($t = 0.005$), (b) $d = 0.024$ ($t = 0.11$), (c) $d = 0.310$ ($t = 0.6$) and (d) $d = 0.88$ ($t = 1.2$). Vorticity contours and two streamlines (thick solid lines) are shown. The center of rotation (x_c, y_c), position of the core vorticity maximum (x_m, y_m), corresponding vorticities ω_c and ω_m, and vortex size s_ψ are indicated in plot (d).

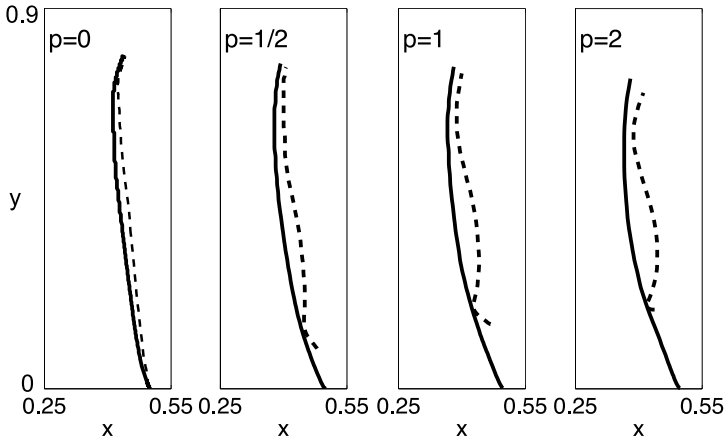

FIG. 9. Trajectories of the rotation center (x_c, y_c) (solid line) and the position of the vorticity maximum (x_m, y_m) (dashed line) for various p, as indicated, for $d \in [0, 3]$.

region. Their values converge as h decreases to curves given by

$$T_R \approx 0.15p^3, \quad T_M \approx 1.5p^2, \tag{10}$$

showing that they both vanish as $p \to 0$, and that T_R decreases at a faster rate than T_M. These results are consistent with the observations for impulsively started flow ($p = 0$) in Ref. 10, in which a recirculation region enclosing a vorticity maximum was visible practically from the beginning of the motion, in time $O(\Delta t)$. Thus, the Rayleigh stage is absent for impulsively started flow and grows as p increases.

E. Inviscid scaling: Core trajectory and circulation

Scaling laws are known to govern the spiral roll-up of an inviscid vortex sheet model for a shear layer, in the absence of an external length scale. Using dimensional analysis, Kaden[6] derives self-similar scaling laws for the roll-up of a semi-infinite vortex sheet. Pullin[7] considers the vortex sheet separating at the edge of a semi-infinite plate, driven by an accelerating background flow $\widehat{\psi}_\infty = A\widehat{t}^p\widehat{r}^{1/2}\cos(\theta/2)$, where $\widehat{r}, \theta$ are polar coordinates centered on the plate tip and A is a dimensional constant. He found the scaling governing the separated vortex sheet roll-up and computed

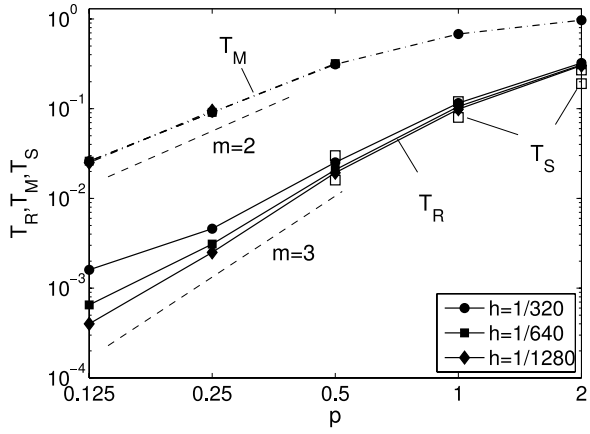

FIG. 10. The duration T_R of the Rayleigh stage (—) and the time T_M at which the core vorticity maximum appears (-.) are shown for $p \in [0.125, 2]$, computed with three resolutions $h = 1/320, 1/640, h = 1/1280$. The dashed lines have the indicated slope m. The square symbols (□) denote the times T_S defined in Sec. IV E.

its time-independent self-similar shape. He also considered vortex sheet separation past wedges of angle $\beta > 0°$. For $\beta = 0$, Pullin's results show that the (dimensional) spiral center coordinates and the shed circulation satisfy

$$\widehat{x}_c + i\widehat{y}_c \approx \Omega_0\Big(\frac{A\widehat{t}^{1+p}}{1+p}\Big)^{2/3},\ \widehat{\Gamma} \approx J\frac{A^{4/3}\widehat{t}^{\frac{1+4p}{3}}}{(1+p)^{1/3}}, \tag{11}$$

where the complex number Ω_0 and J depend weakly on p. In the dimensionless variables used here, with $\widehat{x}_c = L(0.5 - x_c)$, $\widehat{y}_c = Ly_c$, $\widehat{t} = Tt$, and setting $A = L^{1/2}a$, corresponding to potential flow past the finite plate, the self-similar scaling (11) implies that the vortex displacement from the tip and its circulation satisfy

$$(x_c - 0.5) + iy_c \approx Cd^{2/3},\ \Gamma \approx J(1+p)^{\gamma\alpha}d^{\alpha}, \tag{12}$$

where $\alpha = \frac{1+4p}{3(1+p)}$ and $\gamma = 1 - \frac{1}{3\alpha}$. Previously,[10] we found that for $p = 0$, Eq. (12) is closely satisfied over several decades in time. Here, we investigate the accelerated case, for which the situation is less transparent.

We first compare the numerical results with the experimental measurements of Pullin and Perry[4] and the corresponding inviscid similarity theory. Figure 11 reproduces the data presented in their Figure 3 for accelerated flow past a wedge with angle $\beta = 5°$, acceleration parameter $p = 0.45$, and $Re = 6621$, as well as results from our simulations of this case. It shows the vortex center coordinates $\widehat{x}, \widehat{y}$ relative to the plate tip, as a function of time. Consistent with the rest of this paper, $\widehat{x}$ refers to the vortex displacement parallel to the plate, while $\widehat{y}$ refers to the displacement normal to the plate. The experimental data, denoted by open and solid circles, are the coordinates of the center of the spiral streakline reproduced in Figure 7 above, left column. The thick and thin dashed curves denote the similarity theory results for the $\beta = 5°$ case. The thick and thin solid curves show the computed coordinates of the rotation center using our simulations for $\beta = 0°$, with $p = 0.45$, $Re = 6000$.

The data are shown until $\widehat{t} = 6$, which corresponds to nondimensional time and displacement $t \approx 0.58$ and $d \approx 0.31$. At these times, the vortex center still travels towards the axis, with decreasing values of x_c. The figure shows excellent agreement of the computed values of $\widehat{y}$ with both the experimental data and the inviscid theory, for relatively long times $\widehat{t} \le 3$. After this time, all three values begin to differ, indicating that the finite plate length and possibly the wedge angle and the physical wall along the centerline begin to affect the results. The computed values of $\widehat{x}$ are in very good agreement with the similarity theory results, as much as visible on this linear scale.

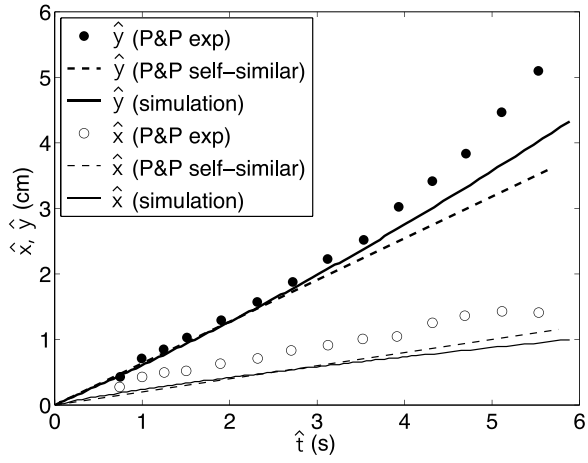

FIG. 11. Comparison of dimensional vortex core coordinates $(\widehat{x}, \widehat{y})$ relative to the plate tip, for $p = 0.45$. Experimental results of Pullin and Perry[4] ($Re = 6621$, $\beta = 5°$), inviscid similarity theory results,[4,7] and numerical results for the rotation center ($Re = 6000$) are shown.

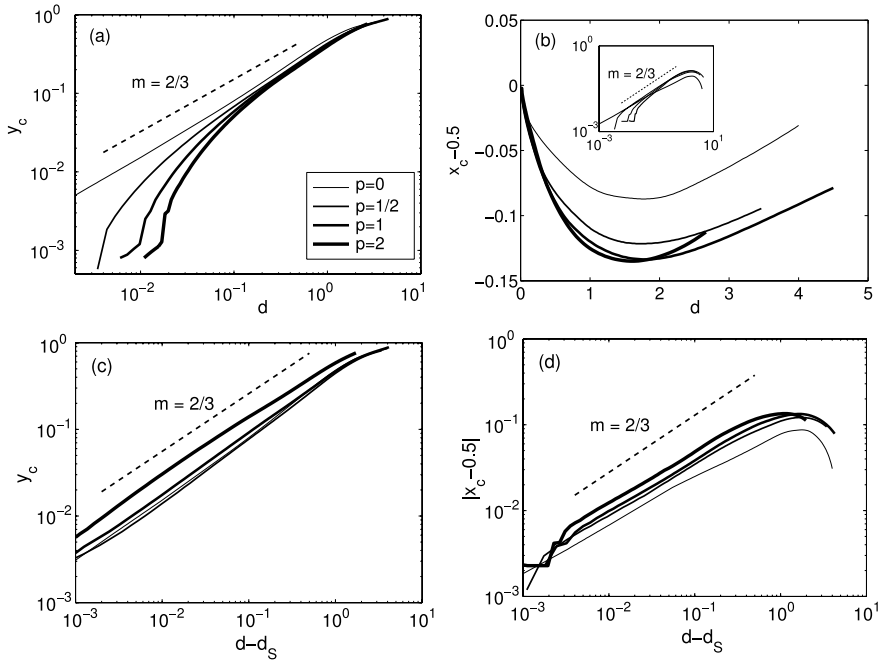

FIG. 12. (a) and (b) Coordinates of the rotation center, *vs.* displacement d. (c) and (d) Coordinates of the rotation center, *vs.* shifted displacement $d - d_S$, where $d_S = d(T_S)$. Results are shown for $p = 0, 1/2, 1, 2$, as indicated in the legend in (a). The dashed lines have the indicated slopes.

Figure 12 compares the computed data with inviscid similarity theory over a larger range of times, for several values of $p \in [0,2]$. Figures 12(a) and 12(b) plot the computed coordinates $x_c - 0.5$ and y_c of the rotation center as a function of the displacement d. We note that with regards to self-similar scaling, the coordinates (x_m, y_m) of the core vorticity maximum are of less interest and not shown here, since for $p > 0$, the maximum is not defined early on, and, once defined, its trajectory oscillates without following clear scaling laws. Figure 12(a) shows that for $p = 0$, y_c closely satisfies the scaling of the inviscid flow, over several decades in time. However, for $p > 0$, there is a large transition region during approximately $d < 0.2$, in which y_c slowly approximates the inviscid scaling. The horizontal displacement $x_c - 0.5$ shown in Figure 12(b) first decreases as the vortex moves towards the axis, and then increases around $d = 1.5$ as the vortex moves outward. The inset, in which $|x_c - 0.5|$ is plotted on a logarithmic scale, shows that during the inward motion, the inviscid scaling is fairly well satisfied for $p = 0$, while for $p > 0$, it again appears to hold after an initial transition period.

The transition period evident in Figures 12(a) and 12(b) in which the data with $p > 0$ do not yet satisfy the inviscid scaling may be thought to represent the second viscous stage in the proposed four-stage vortex evolution. To better estimate the beginning of the self-similar stage, Figures 12(c) and 12(d) plot y_c and $x_c - 0.5$ as a function of a shifted variable $d - d_S$, where $d_S = d(T_S)$ for some time T_S chosen so that the curves appear linear in this logarithmic scale. We note that the curves closely satisfy the self-similar scaling over about four decades in the variable $d - d_S$. The times T_S are plotted in Figure 10 as open squares for the three values of $p > 0$ presented in Figure 12(c) and 12(d). We draw two conclusions:

1. Note that the values of T_S are small, with the corresponding values of $d_S \le 0.005$. For large values of $d - d_S$, it follows that $d - d_S \approx d$. We observe that: the scaling of y_c holds very well until $d = 1$; the scaling of x_c holds well until $d = 0.5$ to 1, depending on the value of p.
2. Note that $T_S \approx T_R$. This implies that the self-similar stage begins practically at the end of the first Rayleigh stage, which ends at $t = T_R$. This in turn implies that the second viscous stage is practically absent.

Next, we present the scaling of the shed circulation Γ as a function of p, where Γ is the integral of the separated vorticity. We first define the region of separated vorticity for times $t > T_R$, at which a recirculation region and associate negative vorticity has formed near the tip. Shortly after $t = T_R$, the vorticity contours are as shown in Figure 13(a). In particular, the contours above the plate contain a characteristic point of maximal curvature. These high curvature points closely follow a slant line to the left of the vortex. Following our earlier work,[10,20] we define the shed circulation to be

$$\Gamma(t) = \int_{\Omega(t)} \omega(\cdot,t)dA, \tag{13}$$

where Ω is as shown in Figure 13(a). It includes all positive vorticity to the right of the slant line and all vorticity to the right of the tip. The negative vorticity attached to the wall is excluded, although it is included at later times, when it has convected into Ω through $x = 0.5$.

For $t < T_R$, it is less clear how to define shed circulation. Figure 13(b) therefore plots the circulation Γ, as a function of the displacement d, for $t \geq t_R$, for all $p = 0, 1/2, 1, 2$. For each p, the curves closely follow a straight line in the logarithmic scale shown, indicating a power law behaviour $\Gamma \sim d^q$. The slopes q increase with increasing p. To better compare the present results with inviscid scaling (12). Figure 13(c) plots $\Gamma^{1/\alpha}/(1+p)^{\gamma}$ vs the displacement d. The curves for all p are almost parallel and have slope approximately equal to 1, showing that

$$\frac{\Gamma^{1/\alpha}}{(1+p)^{\gamma}} \approx d$$

and thus, that the power law scaling (12) is closely satisfied. Furthermore, the scaling is closely satisfied to within $d = 0.5$ to 1, depending on the value of p. We conclude that the inviscid scaling

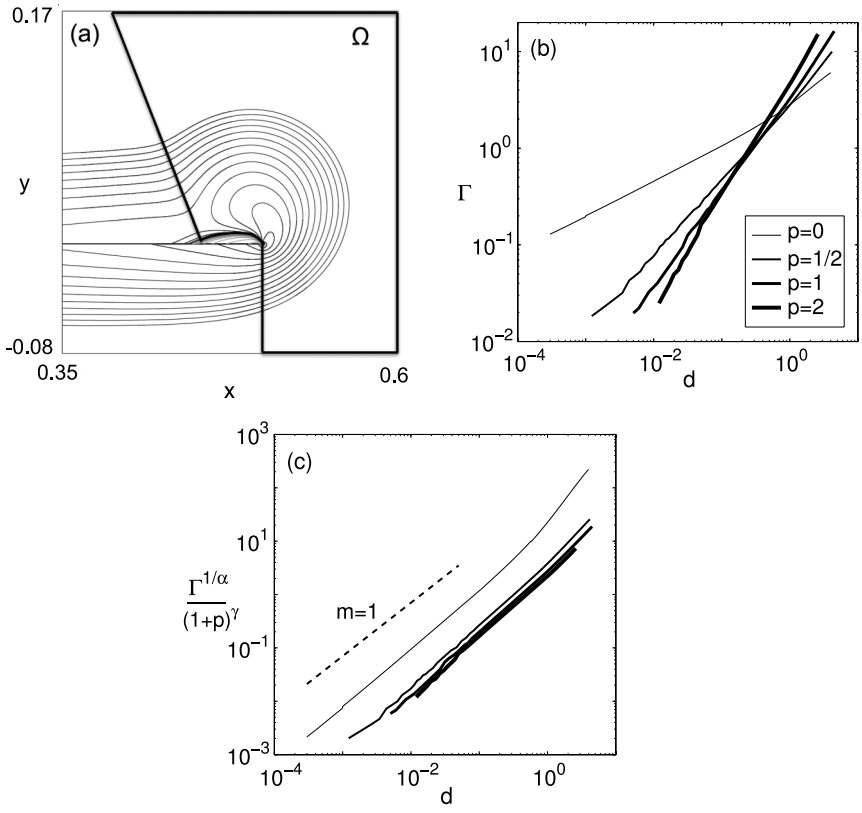

FIG. 13. (a) Sketch showing domain Ω used to define shed circulation Γ, following Ref. 20 (b) Γ vs displacement d. (c) $\Gamma^{1/\alpha}/(1+p)^{\gamma}$ vs d. Where $\alpha = \frac{1+4p}{3(1+p)}$, $\gamma = \frac{3p}{1+4p}$. Results are shown for $p = 0$, 1/2, 1 and 2, as indicated in (b). The dashed line in (c) has the indicated slope.

holds starting from the end of the Rayleigh stage, until the plate displacement is 0.5 to 1 times its length.

F. Viscous scaling: Boundary layer and core vorticity

In the absence of an external length scale, dimensional analysis of viscous flow suggests a self-similar form for the flow stream function,

$$\widehat{\psi}(\widehat{x},\widehat{y}) = A\widehat{t}^{\,p}(\nu\widehat{t})^{1/4} f\Big(\frac{\widehat{x}}{\sqrt{\nu\widehat{t}}},\frac{\widehat{y}}{\sqrt{\nu\widehat{t}}}\Big), \tag{14}$$

which holds globally only if initial and boundary conditions can be satisfied with this ansatz. This self-similar form implies that length scales, such as the boundary or shear layer thickness, and fluid vorticity scale as

$$\hat{\delta} \sim \sqrt{\nu\widehat{t}}, \quad \widehat{\omega} \sim A\widehat{t}^{\,p}(\nu\widehat{t})^{-3/4}. \tag{15}$$

In our nondimensional variables, using $A = L^{1/2}a$, the corresponding scaling is

$$\delta \sim \sqrt{t/Re}, \quad \text{or} \quad \delta^{p+1} \sim \sqrt{d}, \tag{16a}$$

$$\omega \sim t^p\Big(\frac{t}{Re}\Big)^{-3/4} \sim d^{\frac{p-3/4}{p+1}} = d^m, \tag{16b}$$

where $m = -3/4, -1/6, 1/8, 5/12$ for $p = 0, 1/2, 1, 2$, respectively. In Ref. 10, we showed that for $p = 0$, the scaling holds locally in certain regions of the flow such as the boundary layer, the vortex center, and the separated shear layer, for several decades in time. Here, we consider $p > 0$.

Figure 14 plots the boundary layer thickness δ and the vorticity ω_c and ω_m, for $p \geq 0$, as functions of the displacement d. Figure 14(a) plots δ^{p+1}, where δ is the vertical thickness of the region below the plate with $\omega \geq 2^{-12}$, at $x = 0.25$. Results for other values of x are qualitatively similar. The thickness decreases noticeably as p increases but closely satisfies the viscous scaling in Eq. (15), for all p. The scaling holds for approximately $d \in [0, 0.1 \text{ to } 0.3]$ and holds slightly longer for smaller values of p.

Figure 14(b) plots ω_c *vs.* d and dashed lines with the indicated slopes. While the viscous scaling (15) holds for $p = 0$ over several decades in d, it is observed over a much smaller time interval for $p > 0$, and only after an initial transition region. The core vorticity maximum ω_m, plotted in Figure 14(c), exists only at relatively large times, $t > T_M$, and does not satisfy the viscous scaling (15). We conclude that the boundary layer thickness satisfies the viscous scaling during much of the inviscid self-similar regime, but for $p > 0$, the core vorticity is not clearly predicted by dimensional analysis.

G. Comparison with simulation

This last section presents a comparison with existing numerical results of Koumoutsakos and Shiels,[5] at somewhat larger times. The vortex size s_Ψ is defined in Figure 8(d) as the height of the recirculation region on the axis of symmetry along the middle of the plate. Note that this quantity

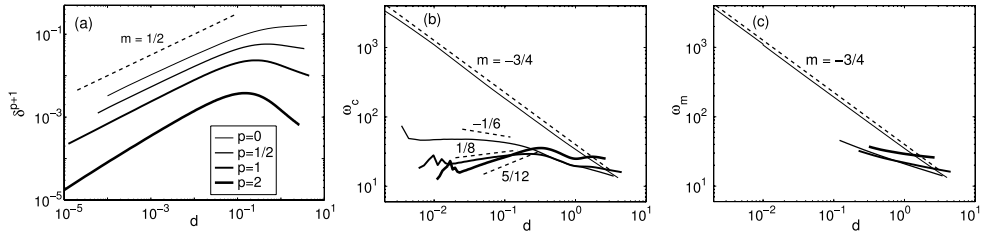

FIG. 14. (a) Boundary layer thickness δ, (b) Vorticity ω_c at the center of rotation. (c) Maximum core vorticity ω_m. Results for $p = 0, 1/2, 1$ and 2, are shown, as indicated. The dashed lines have the indicated slope.

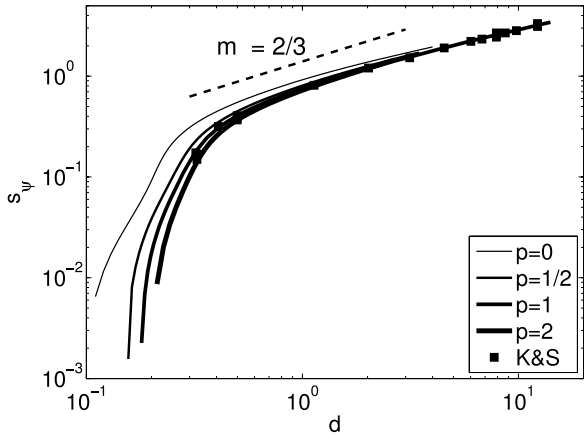

FIG. 15. Vortex size s_ψ vs. displacement d, for $p = 0, 1/2$, 1 and 2, as indicated. The data computed by Koumoutsakos and Shiels[5] for $p = 1$ are shown as black squares. The dashed line has the indicated slope.

is defined only after the recirculation region has formed and has reached the axis of symmetry, as, for example, in Figure 8(c). It is thus not defined at early times and cannot scale as a power law early on, but it was observed by Taneda and Honji[3] to approximately scale at intermediate times. Koumoutsakos and Shiels[5] computed s_ψ for $p = 1$ and several values of Re and found good agreement with these earlier experimental data. Figure 15 plots our computed values of s_Ψ for all values of p, as a function of d, together with the values for $p = 1$ presented by Koumoutsakos and Shiels.[5] Note that our values for $p = 1$ are in excellent agreement with those of Ref. 5. Furthermore, as a function of d, all curves with different values of the acceleration parameter p approach the same common curve. In turn, this curve satisfies the scaling law $s_\Psi \sim d^{2/3}$ at intermediate times. We conclude that s_Ψ is most concisely described in terms of the displacement d instead of time t, and that s_Ψ closely follows the scaling $d^{2/3}$ at intermediate times, independently of the acceleration parameter p. The initial transition period is not a viscous or finite plate effect and thus the scaling does not hold asymptotically as $d \to 0$ in any particular limit. The size does reflect the growth of the vertical vortex displacement y_c, which also scales as $d^{2/3}$.

V. SUMMARY

This paper presents numerical simulations of viscous starting flow past a finite flat plate moving with accelerated velocity $U = t^p$ ($\widehat{U} = a\widehat{t^p}$) in the direction normal to itself. The focus is on the effect of the parameter p, for $p = 0, 1/2, 1, 2$, for fixed value of the Reynolds number, $Re = 500$. The main contributions are to resolve the flow at early times, compute quantities such as vortex trajectory and circulation over several decades in time, and report new features present for $p > 0$ which are not present for $p = 0$. Most results are reported as functions of the plate displacement d, which more concisely reflect the dependence on p.

The main results can be summarized in a three-stage framework, which in essence quantifies and evaluates the one proposed by Luchini and Tognaccini:[11]

- **Stage 1: Rayleigh layer.** The initial flow consists of a viscous boundary layer of vorticity of approximately uniform thickness surrounding the plate and the plate tip and does not contain any separated streamlines. We show that the stage is only present for $p > 0$ and lasts for a time T_R that scales like p^3, as $p \to 0$. The Rayleigh stage ends at $t = T_R$, when a recirculation region has formed near the plate tip.
- **Stage 2: Self-similar growth.** There are two scalings that are relevant at times when the vortex is small relative to the plate length: inviscid scaling laws known to hold for a vortex sheet model of the flow in the absence of a length scale, and viscous laws that hold for self-similar viscous flows. In stage 2, several quantities grow following either the inviscid or

viscous scaling laws. The inviscid self-similar growth lasts until the plate has moved by about $d = 0.5$ to 1 times the plate length, depending on the value of p. The rotation center and the vortex circulation follow the inviscid scaling laws over several decades in time. The extent to which these laws apply to viscous flows was previously unknown. The rotation center scales self-similarly as a function of a shifted time $t - T_S$, where $T_S \approx T_R$. That is, the transition from the Rayleigh stage to the self-similar stage is immediate, with no apparent intermediate stage. The boundary layer thickness satisfies viscous scaling laws throughout most of stage 2. Unlike the $p = 0$ case, for $p > 0$, the vorticity at the rotation center satisfies viscous scaling laws only over a small time-interval. Also unlike the $p = 0$ case, for $p > 0$, the core vorticity maximum occurs much after the recirculation region forms and does not satisfy any apparent scaling.

- **Stage 3: Finite plate effects.** After the end of stage 2, approximately when $d = 0.5$ to 1, the finite plate geometry is no longer negligible and departs from self-similar growth.

The results are also compared with experimental results of Pullin and Perry[4] and numerical results of Koumoutsakos and Shiels.[5] The comparisons yield additional information on secondary separation in flow past thin wedges and on the effect of underresolution on the onset of instabilities.

ACKNOWLEDGMENTS

We thank anonymous reviewers for helpful comments and suggestions that improved the paper. We also thank Robert Krasny for many useful discussions.

[1] J. D. Anderson, Jr., "Ludwig Prandtls boundary layer," Phys. Today **58**(12), 42–48 (2005).
[2] H. J. Lugt, *Introduction to Vortex Theory* (Vortex Flow Press, Potomac, MD, 1996).
[3] S. Taneda and H. Honji, "Unsteady flow past a flat plate normal to the direction of motion," J. Phys. Soc. Jpn. **30**, 262–272 (1971).
[4] D. I. Pullin and A. E. Perry, "Some flow visualization experiments on the starting vortex," J. Fluid Mech. **97**, 239–255 (1980).
[5] P. Koumoutsakos and D. Shiels, "Simulations of the viscous flow normal to an impulsively started and uniformly accelerated flat plate," J. Fluid Mech. **328**, 177–227 (1996).
[6] H. Kaden, "Aufwicklung einer unstabilen Unstetigkeitsfläche," Ing.-Arch. **2**, 140-168 (1931), NASA Technical Translation: Curling of an unstable discontinuity surface, NASA-TT-F-14230, p. 51, 1971.
[7] D. I. Pullin, "The large-scale structure of unsteady self-similar rolled-up vortex sheets," J. Fluid Mech. **88**, 401–430 (1978).
[8] J. Kriegseis, M. Kinzel, and D. E. Rival, "On the persistence of memory: Do initial conditions impact vortex formation?," J. Fluid Mech. **736**, 91–106 (2013).
[9] M. J. Ringuette, M. Milano, and M. Gharib, "Role of the tip vortex in the force generation of low aspect-ratio normal flat plates," J. Fluid Mech. **581**, 453-468 (2007).
[10] L. Xu and M. Nitsche, "Scaling behaviour in impulsively started viscous flow past a finite flat plate," J. Fluid Mech. **756**, 689-715 (2014).
[11] P. Luchini and R. Tognaccini, "The start-up vortex issuing from a semi-infinite flat plate," J. Fluid Mech. **455**, 175–193 (2002).
[12] D. Pierce, "Photographic evidence of the formation and growth of vorticity behind plates accelerated from rest in still air," J. Fluid Mech. **11**, 460–464 (1961).
[13] Q. X. Lian and Z. Huang, "Starting flow and structure of the starting vortex behind bluff bodies with sharp edges," Exp. Fluids **8**, 95–103 (1989).
[14] Z. J. Wang, J. G. Liu, and S. Childress, "Connection between corner vortices and shear layer instability in flow past an ellipse," Phys. Fluids **11**, 2446–2448 (1999).
[15] K. Schneider, M. Paget-Goy, A. Verga, and M. Farge, "Numerical simulation of flows past flat plates using volume penalization," Comput. Appl. Math. **33**, 481–495 (2014).
[16] C. Lepage, T. Leweke, and A. Verga, "Spiral shear layers: Roll-up and incipient instability," Phys. Fluids **17**, 031705 (2005).
[17] W. E and J. G. Liu, "Essentially compact schemes for unsteady viscous incompressible flows," J. Comput. Phys. **126**, 122-138 (1996).
[18] L. Xu, "Viscous flow past flat plates," Ph.D. thesis (University of New Mexico, 2012).
[19] D. L. Brown and M. L. Minion, "Performance of under-resolved two-dimensional incompressible flow simulations," J. Comput. Phys. **122**(1), 165-183 (1995).
[20] M. Nitsche and L. Xu, "Circulation shedding in viscous starting flow past a flat plate," Fluid Dyn. Res. **46**, 061420 (2014).